ACS Sustainable Chemistry & Engineering

Research Article

pubs.acs.org/journal/ascecg

Microcellular Electrode Material for Microbial Bioelectrochemical Systems Synthesized by Hydrothermal Carbonization of Biomass Derived Precursors

Victoria Flexer,[*,†,○] Bogdan C. Donose,[†,△] Camille Lefebvre,[†] Guillermo Pozo,[†] Matthieu N. Boone,[‡] Luc Van Hoorebeke,[‡] Mohamed Baccour,[§] Laurent Bonnet,[∥] Sylvie Calas-Etienne,[∥] Anne Galarneau,[§] Magdalena M. Titirici,[⊥] and Nicolas Brun[*,§]

[†]Advanced Water Management Centre, The University of Queensland, Level 4, Gehrmann Building (60), Brisbane, QLD 4072, Australia

[‡]Centre for X-ray Tomography, Department of Physics and Astronomy, Ghent University, Proeftuinstraat 86, B-9000 Gent, Belgium

[§]Institut Charles Gerhardt de Montpellier, UMR 5253, CNRS-ENSCM-UM, Université de Montpellier, CC 1701, Place Eugène Bataillon, 34095 Montpellier, France

[∥]Laboratoire Charles Coulomb, UMR 5221, CNRS-UM, Université de Montpellier, CC 069, Place Eugène Bataillon, 34095 Montpellier, France

[⊥]School of Engineering and Materials Science, Queen Mary University of London, Mile End Road, E14NS, London, United Kingdom

Supporting Information

ABSTRACT: A new monolithic carbonaceous material, 750-HMF-CarboHIPE, is presented here. The new electrode has been tested as an anode material inside a microbial bioelectrochemical system. In a purposely designed continuous flow bioelectrochemical reactor, the new material showed high biocompatibility, with a continuous biofilm development that remained bioelectrochemically active for over 6 months. A catalytic current of 1.56 mA cm^{-2}/7.8 mA cm^{-3} (normalization by projected surface area and volumetric current) was reached. The current density was proportional to the flow rate. The new electrode material was synthesized using a high internal phase emulsion (HIPE) as a soft template to confine the polymerization and hydrothermal carbonization of two precursors derived from the cellulosic fraction of biomass and the bark of fruit trees: 5-hydroxymethylfurfural and phloroglucinol, respectively. Altogether, the sustainable synthetic route from biomass materials and the proposed application of oxidizing organic matter present in wastewater to produce electricity in a microbial fuel cell (MFC) close an interesting loop of prospective sustainable technology.

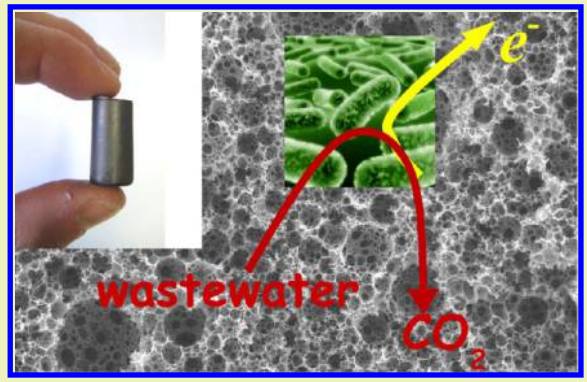

KEYWORDS: *Microbial bioelectrochemical systems, microbial fuel cells, electrochemically active biofilm, electrode material, porous carbons*

INTRODUCTION

Carbon-based materials can be used in a wide variety of applications, thanks to a relative low cost and inherent attractive properties, such as high surface area, chemical inertness, thermal stability and electrical conductivity.[1−4] Porous carbons have been applied as adsorbents,[5,6] electrodes,[1,7] catalytic,[4,8] or electrocatalytic supports,[9−11] or even as intrinsic electrocatalysts.[12,13] In particular, macroporous carbons, exhibiting pores diameters larger than 50 nm within an interconnected framework, are promising as they present many structural advantages.[9,11] Macropores increase the accessibility of the bulk and the associated active surface (i.e., smaller pores, functional groups, immobilized or adsorbed catalysts), while improving the mass transport rate through the whole porous network. This fact is particularly important when the desired application involves either the immobilization of bulky catalysts, such as large particles, proteins, bacteria, etc., or when the application requires the use of continuous flow set-ups in liquid media to limit pressure drop. Therefore, hierarchical macroporous carbons have recently been employed for the design of enzyme-based electrodes for bioelectrocatalysis and biofuel cells. Among synthetic pathways used to prepare macroporous materials, the polymerization of the continuous phase of high internal phase emulsions (HIPEs) have been largely exploited.[13−15] In particular, the design of biosourced emulsion-templated carbons was recently proposed by some

Received: November 29, 2015
Revised: February 25, 2016
Published: March 17, 2016

DOI: 10.1021/acssuschemeng.5b01592
ACS Sustainable Chem. Eng. 2016, 4, 2508−2516

of us.[9,12] These novel foams, named carboHIPEs, complied most of the requirements in terms of functionality, easy design and shaping, and sustainability, necessary for many environmentally friendly applications. Actually, such microcellular monoliths were synthesized through the hydrothermal carbonization (HTC) of biomass derived precursors. Within the field of sustainable carbon materials, HTC has emerged this past decade as a prevalent approach.[16,17] It allows for condensation, shaping, and structuration of carbonaceous materials in water or hydroalcoholic mixtures at relatively mild conditions (typically temperatures between 130 and 250 °C). Interestingly, various templating strategies, such as emulsions, have been developed to design porous HTC materials. HTC is based on the degradation/dehydration of saccharides into furan-based intermediates, leading after nucleation/growth to carbon-like colloidal spheres, termed HTC materials or hydrochars. Typically, monosaccharides are employed as precursors. However, in a practical way HTC can be easily extended to wet impure precursors, raw biomass, and biowastes. As for carboHIPEs, 5-(hydroxymethyl)furfural (5-HMF), a saccharide derivative, and phloroglucinol were used as precursors. While 5-HMF can be isolated from the cellulosic fraction of lignocellulosic biomass, phloroglucinol can be extracted from the bark of fruit trees. These biomass derivatives avoid the use of synthetic resorcinol/formaldehyde precursors and divinylbenzene-based polymers and constitute an alternative green route for the synthesis of carbon electrodes.

Notably, carboHIPEs were successfully used as bioelectrodes for the enzymatic oxidation of glucose.[9] These preliminary results gave a hint of the potential use of biosourced carboHIPEs as electrodes in biofuel cells.

The biofuel cell technology can be seen as a versatile and sustainable alternative for electricity generation in some specific applications. Biofuel cells employ active bioentities (enzymes or bacteria) to convert environmentally friendly biomass or biofuels into "green" electrical power. In microbial bioelectrochemical systems (BES), whole cells are used as biocatalysts to catalyze oxidation and reduction reactions.[18−22] Microbial fuel cells (MFCs) are the classical and pioneer example of bioelectrochemical systems, performing the double task of wastewater treatment and electricity generation.[18−20] The organic matter present in wastewater becomes the fuel to be oxidized all the way from multicarbon compounds to CO_2. In addition, the possibility of synthesizing higher value products from CO_2 or short chain carbon compounds at the cathode of a BES was recently envisioned and has become an interesting candidate technology for the sustainable production of fuels and chemicals.[21−24] The economic feasibility and prospective industrial application of these systems is highly dependent on performance improvement, particularly increased electrical currents.[25−27] Current production is dependent on several parameters, most notably: the starting microbial community, the reactor design, the operating conditions, and the electrode materials.[26,28] While the first three parameters have been widely studied for more than a decade, until not long ago, the electrode material design was hardly ever considered, and commercially available carbonaceous materials,[18] such as carbon felt, carbon cloth, carbon paper, and graphite granules or rods, were employed almost exclusively in the field. The research toward improved electrode materials, purposely designed for microbial bioelectrochemical applications is relatively recent.[29−36] The general approach aims at increasing the active surface area available for biofilm growth by creating roughness on the electrode and/or macroporosity. Another strategy aims at designing materials with specific properties that will improve the bacteria-electrode interaction, and especially the rate of electron transfer.[28]

Great improvements can be imagined for bioelectrochemical systems if three-dimensional anodes and cathodes could be employed. Contrary to rough electrode surfaces or dense fibrous material such as carbon felt or graphite plates or granules, we refer here to true three-dimensional electrodes, where all three geometric dimensions are of the same order of magnitude, and where bacteria will be able to grow in the interior of the three-dimensional structure. Ideally, self-standing three-dimensional materials should bear macropores at least in the tens of micrometer scale in order to allow for efficient mass transport. Multidirectional interconnected pores are desirable to maximize fluid flow toward and out of the pores.[11] In addition to ensuring efficient mass transfer to and from the electrode surface, the macroporosity will drastically increase the accessible surface area of the electrode and therefore the microbial loading. In turn, porosity below known bacterial dimensions (nanopores or below) will help ensure efficient bacterial attachment and might increase the electron transfer rate. Indeed, nanometric features will create more electrical contact points between the bacterial electron transfer entities (nanowires, membrane proteins or soluble shuttles) and the solid electrode surface.[36]

The incorporation of 3D-macroporous (or hierarchical 3D-macroporous) electrode materials resulting from biomass into microbial electrochemical systems is an attractive idea. Indeed, whether we aim at green electricity generation, wastewater treatment, or bioelectrosynthesis from CO_2, we would like to ensure that the synthesis of the electrodes also follows a green route.

Here we report on a new prospective microbial electrode material (750-HMF-CarboHIPE) bearing a hierarchical porous structure synthesized by hydrothermal carbonization of emulsion-templated macroporous carbons. Results show that our new material is highly biocompatible. Uniform and continuous biofilm development was achieved on the outside surface of the electrode as well as within the scaffold. Partial clogging of the pores was observed, suggesting that the macropores size should still be optimized toward larger pores. Despite this clogging, the bacteria were electrically connected to the electrode surface and the bioelectrocatalytic current was stable during six months in continuous operation.

EXPERIMENTAL SECTION

Electrode Synthesis. Dodecane, Tween 80 [polyoxyethylene (20) sorbitan monooleate], iron(III) chloride hexahydrate ($FeCl_3{\cdot}6H_2O$), and 5-(hydroxymethyl)furfural (5-HMF) were purchased from Sigma-Aldrich. Phloroglucinol 99% anhydrous was purchased from Acros Organic.

In a typical synthesis, nonionic surfactant Tween 80 (1 mL) was added in a hydroalcoholic mixture of demineralized water (2.4 mL) and absolute ethanol (2.4 mL). Then, phloroglucinol (0.312 g) and 5-HMF (0.572 g; corresponding to 1 mol equiv of phloroglucinol for 2 equiv of 5-(hydroxymethyl)furfural) were mixed into this solution. After a vigorous stirring for a few minutes, iron(III) chloride hexahydrate (0.1335 g), acting as a Lewis acid catalyst, was added. The solution turned quickly black, due to the soluble polymers generated by fast reaction between the phenolic compound and furan compound. Promptly, the prepolymerised hydroalcoholic solution was put in a mortar and dodecane (23.2 mL) was added drop-by-drop while emulsification was performed manually with a pestle. The

DOI: 10.1021/acssuschemeng.5b01592
ACS Sustainable Chem. Eng. 2016, 4, 2508−2516

volume of dodecane in comparison to the volume of the hydro-alcoholic solution corresponds to an oil volume fraction of 0.8. The as-synthesized viscous emulsion was then added in a glass inlet (30 mL volume) sealed in a Teflon lined autoclave (45 mL volume) and placed in a laboratory oven preheated to 130 °C and left at 130 °C for 24 h. The resulting material named HTC-CarboHIPE was then removed from the autoclave, washed by Soxhlet extraction with ethanol during 24 h and dried at 80 °C in an oven. The dried HTC-CarboHIPE was placed in a ceramic crucible and heated until 750 °C at a rate of 3 °C/min and left at 750 °C for 4 h under an inert atmosphere (i.e., N_2 flow 10 mL min^{-1}). The sample was then allowed to cooled to ambient temperature in the oven. The resulting cellular porous carbon was then named 750-HMF-CarboHIPE. Finally, materials were shaped by cutting into the desired shape for the electrochemical reactor setup, i.e. into cylindrical monoliths pellets of 0.2 cm thickness and 1.26 cm diameter to form the electrodes.

Bioelectrochemical Experiments. The electrodes were tested in a membraneless purposely designed electrochemical reactor, made of Perspex (Figure S1). The first half consisted of a cylindrical compartment, with a bore 1.16 cm diameter, 1.8 cm high, ending in a 1 mm wide step at the top that widens to 1.26 cm, and is 2 mm high, were the working electrode sits. A stainless steel ring, with an electrical connection to the outside ensures the electrical contact with the working electrode. This contact is reinforced by conductive carbon paint. An epoxy resin was used to seal the electrode against the border of the reactor to ensure that both the inoculum and the feed go only through the macropores of the electrode material and not in the space between the electrode and the reactor. There is a lateral compartment for the reference electrode. The counter electrode mesh sits in between two bored 1 mm rubber sheets which avoid leakages. The upper compartment has one simple bore, 1.26 cm wide, 2 cm high. The two pieces are screwed tightly together to avoid leakages. The reactor has an inlet in the bottom and an outlet at the top that allows for continuous mode operation. A Ag/AgCl (saturated KCl) reference electrode (CH Instruments, USA) was used and all potentials reported here are referred to this electrode. A large area Ti mesh (1.26 cm^2 footprint, 0.05 mm mesh-spacing) was used as a counter electrode.

Three replicate reactors were inoculated and run independently. All three reactors showed very similar results, with comparable maximum currents reached, similar time lapses to develop current and comparable CV shapes. Because neither current vs time curves, nor CVs can be averaged, only the results of one of the reactors are graphically shown throughout the text.

Once set up in the reactor, the working electrode was pretreated in a N_2 plasma to increase the electrode hydrophilicity and increase the amount of N functionalities, as previously shown by XPS.[37]

All solutions were bubbled with N_2 gas for 30 min (anoxic conditions). The electrode was introduced in the bioelectrochemical reactor and a solution of M9 medium without acetate was pumped continuously at 0.25 mL min^{-1}. After 4 h of pumping, the background signal for cyclic voltammograms (CVs) was measured (6 cycles, 0.1 mV s^{-1}). After CVs, a chronoamperometry experiment was started at an applied potential of 0 V. The background current was measured prior to inoculation for 36 h. The reactor was then inoculated with a mixture of 50 mL anodic effluent of an acclimatized bioelectrochemical reactor at The University of Queensland,[38] and 50 mL of M9 media. This inoculum was pumped at 1 mL h^{-1}. Time 0 corresponds to the start of the inoculation. After inoculation, the reactor was fed continuously with M9 medium and 20 mM acetate. The pumping rate was varied several times during the experiment, as specified in the Results section.

CVs in the presence of 20 mM acetate (turnover conditions) were measured at day 100. Six consecutive CVs were measured; the last three scans showed reproducible results. At the end of the chronoamperometry experiment, fresh media without acetate was pumped for 36 h, after which 6 CVs in the absence of acetate (nonturnover conditions) were measured; the last four scans showed reproducible scans. All CVs were recorded at a scan rate of 0.1 mV s^{-1}.

A Biologic VSP multichannel potentiostat was used for all experiments. A constant potential of 0 V was applied to the anode for the total duration of the experiment, and was always on except for short periods of time when adjustments were made to the pumping system. The medium used was a modified M9 medium (pH = 7.0) with 20 mM sodium acetate as the electron donor, containing 6 g L^{-1} Na_2HPO_4, 3 g L^{-1} KH_2PO_4, 0.1 g L^{-1} NH_4Cl, 0.5 g L^{-1} NaCl, 0.1 g L^{-1} $MgSO_4{\cdot}7H_2O$, 14.6 mg L^{-1} $CaCl_2$, and 1 mL L^{-1} of a mixed trace element solution described elsewhere.[39]

Experiments were run at room temperature 20 ± 3 °C. The reported current values have been normalized by the projected surface area of the electrode (footprint). The current density at maximum flow rate was also normalized by the volume of the electrode. The reactor and all the pumping system were kept in the dark to avoid development of phototroph organisms.

Characterization. N_2 sorption analysis was performed at 77 K using a Micromeritics Tristar 3000, equipped with automated surface area and pore size analyzer. This analysis was performed to measure specific BET surface area, meso- and/or microporous volumes. Before analysis, samples were degassed at 250 °C for 7 h using a Micromeritics VacPrep 061 degasser. BET surface area was determined in the relative pressure range P/P_0 range from 0.01 to 0.04.[40] Mercury intrusion porosimetry was performed using a Carlo Erba porosimeter to measure macropore diameter and macroporous volume. The initial measurement was performed using a Pascal 140 porosimeter at low pressure (400 kPa) followed by secondary analysis using a Pascal 240 porosimeter at high pressure (200 MPa). Macropore diameters, D, were determined using the capillary law governing nonwetting liquid penetration into small pores expressed by the Washburn equation (eq 1):[41,42]

$$D = -4\gamma\cos\varphi(1/P_{Hg}) \quad (1)$$

with

- γ being the surface tension of mercury: γ = 0.48 N m^{-1}
- φ being the contact angle: φ = 140°
- and P_{Hg} being the applied pressure to force mercury into the pores

This equation assumes that all pores are cylindrical.

Scanning electron microscope (SEM) images were obtained using a Gemini SEM (Figure 2a), a Hitachi SU3500 SEM with an Ultra-Variable Pressure Detector (Figure 6a), and a XL30 Philips (LaB6 source electron gun) SEM (Figures 6b and c). Biofilm covered samples were rinsed in distilled water and let to dry before imaging.

The electrical conductivity was measured by electrochemical impedance spectroscopy with a range frequency from 5 to 1 MHz

High-resolution X-ray computed tomography (micro-CT) measurements were performed at the high-resolution setup MEDUSA of the Ghent University Centre for X-ray Tomography. This system uses a FeinFocus FXE160.51 transmission tube with changeable target and a Photonic Science VHR camera with thin scintillator for a low energy response. The tomographic reconstruction is performed using Octopus Reconstruction (Inside Matters, Belgium). A region of a large sample of approximately 4 mm × 7 mm × 15 mm was scanned at a voxel size of 6 μm × 6 μm × 6 μm; whereas a small subsample of approximately 2 mm × 2 mm × 4 mm was scanned at a voxel size of 1.6 μm × 1.6 μm × 1.6 μm. All data sets were reconstructed using the Modified Bronnikov Algorithm,[43] as X-ray attenuation was negligible and phase contrast effects were visible. Furthermore, this algorithm offers a drastic improvement of signal-to-noise ratio.[44]

Image analysis was performed on the small sample using Morpho +,[45] an in-house developed 3D analysis software tool. This package allows for a very modular analysis workflow, extensive parametrization of the pores and exporting of the analyzed volume. The original gray scale volume was afterward rendered together with the pore-size analysis data using Volume Graphics VGStudioMax.

RESULTS

The porosity of the carbon monolith, 750-HMF-CarboHIPE, was characterized by nitrogen adsorption at 77 K to examine the micro- and mesoporosity and by scanning electron

DOI: 10.1021/acssuschemeng.5b01592
ACS Sustainable Chem. Eng. 2016, 4, 2508−2516

microscopy (SEM), mercury porosimetry, and X-ray tomography to analyze the macroporosity. The shape of the nitrogen sorption isotherm is of type I according to IUPAC[40] revealing that the skeleton of the material is mainly microporous (pores diameters inferior to 2 nm), as shown in Figure 1 with a

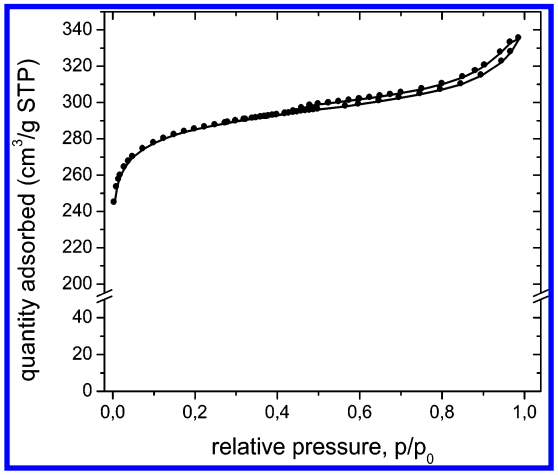

Figure 1. Nitrogen sorption isotherm of the unmodified carbonaceous foam, 750-HMF-CarboHIPE.

microporous volume around 0.43 mL g^{-1}. Even if BET equation cannot be applied for microporous solids due to no multilayer nitrogen adsorption, an equivalent BET surface area for microporous materials can be calculated for materials comparison using the Rouquerol criterium.[42] A high equivalent BET surface area of 1130 m^2 g^{-1} was determined. The surface of the skeleton is rough as evidenced by the slight slope in the nitrogen adsorption after the micropores filling ($0.1 < p/p_0 < 0.8$). A slight hysteresis can be also seen closing at $p/p_0 = 0.47$ revealing that larger pores exist (mesopores and/or narrow macropores), which are connected to the exterior of the solid by the micropores. At the macroscopic scale, the carbon monolith feature a macroporosity typical of emulsion-templated structures showing an aggregation of hollow spheres, usually called *cells*, that can be observed by SEM in Figure 2a. These correspond to the removed soft template itself, i.e. the oil droplets of a direct emulsion. Herein, *cells* with diameters from 10−50 μm were obtained. Thus, the as-synthesized material can be seen as a foam, usually defined as microcellular. In addition to these *cells*, narrower pores of 1−3 μm could be observed by SEM at higher magnification (Figure 2a, inset). It can be assumed that these pores, usually called *connecting windows*, were induced either by the nonpolymerized interstices that remained in the continuous phase of the emulsion or by direct contacts between two nearby packed oil droplets. Mercury intrusion porosimetry seems to reveal only these windows as the mean pore diameter calculated by this technique is around 0.9 μm ($0.2 < D < 1.5$ μm; Figure 2b). It seems that mercury has to penetrate the small windows to access to the macroporous volume. A very large total macroporous volume of 9 mL g^{-1} has been found. Mercury porosimetry gives an equivalent cylindrical diameter for the macropores with the Washburn−Laplace equation, whereas pores in the sample are spherical. This technique seems not adapted to characterize the entire porosity of microcellular materials, however it gives a valuable insight into the size distribution of the connecting windows and the macroporous volume of the sample. At this stage, X-ray tomography (3D-analysis) seems to be more

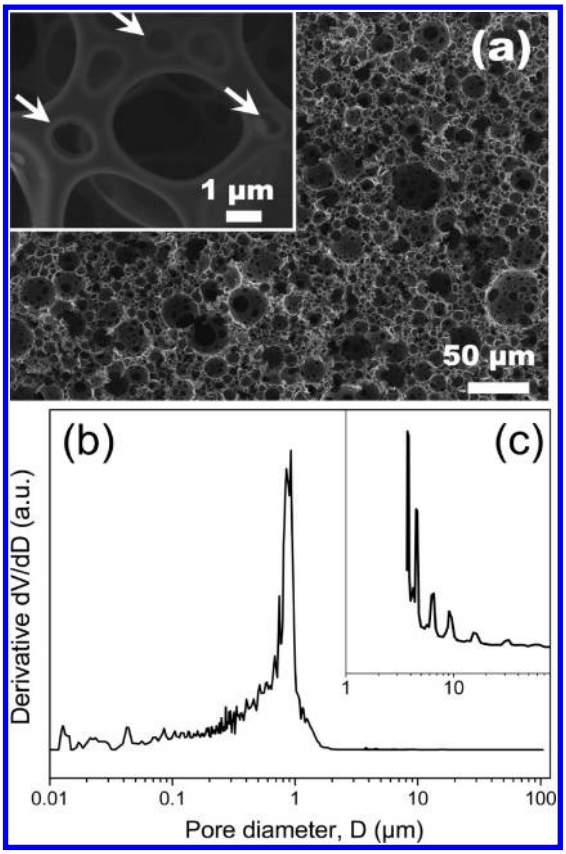

Figure 2. (a) SEM micrographs of the unmodified carbonaceous foam. The white arrows highlight the so-called connecting windows between macroscopic *cells*. (b) Macroscopic pore size distribution obtained by mercury intrusion porosimetry combining measurements performed using a Pascal 240 (up to 200 MPa) and a Pascal 140 (up to 400 KPa). (c) Data obtained at low pressure using a Pascal 140.

adapted to characterize microcellular foams and to provide a global repartition of small and large macropores in addition to SEM.

To the best of our knowledge, X-ray tomography had never been applied to the characterization of carboHIPEs. All these techniques bring together a full picture of the bear materials as it had never been shown before. Due to the limitation of spatial resolution, the 3D analysis of the micro-CT data set is limited to pores larger than ∼2 μm diameter. Furthermore, the absolute values of the results are prone to variations based on the thresholding step which is performed on the gray values. Nevertheless, 3D analysis gives extremely valuable information about the spatial distribution of the pore size distribution throughout the sample,[46] where particularly the bigger pores contribute largely to the heterogeneity of a material. Additionally, the partial volume effect allows for the retrieval of information beyond the limits of the spatial resolution. Indeed, in a homogeneous but porous material, the local X-ray attenuation coefficient is directly proportional to the volume fraction of material in that area, where the area is defined by the spatial resolution of the data set.

Figure 3 shows a combined rendering of the grayscale data with 3D analysis results. From the 3D analysis, no unpredicted properties can be found. The pores are randomly distributed in the volume, with their size normally distributed. The pores are mostly spherical, and consequently no preferential orientation of the pores can be observed. The pores are classified and color-

DOI: 10.1021/acssuschemeng.5b01592
ACS Sustainable Chem. Eng. 2016, 4, 2508−2516

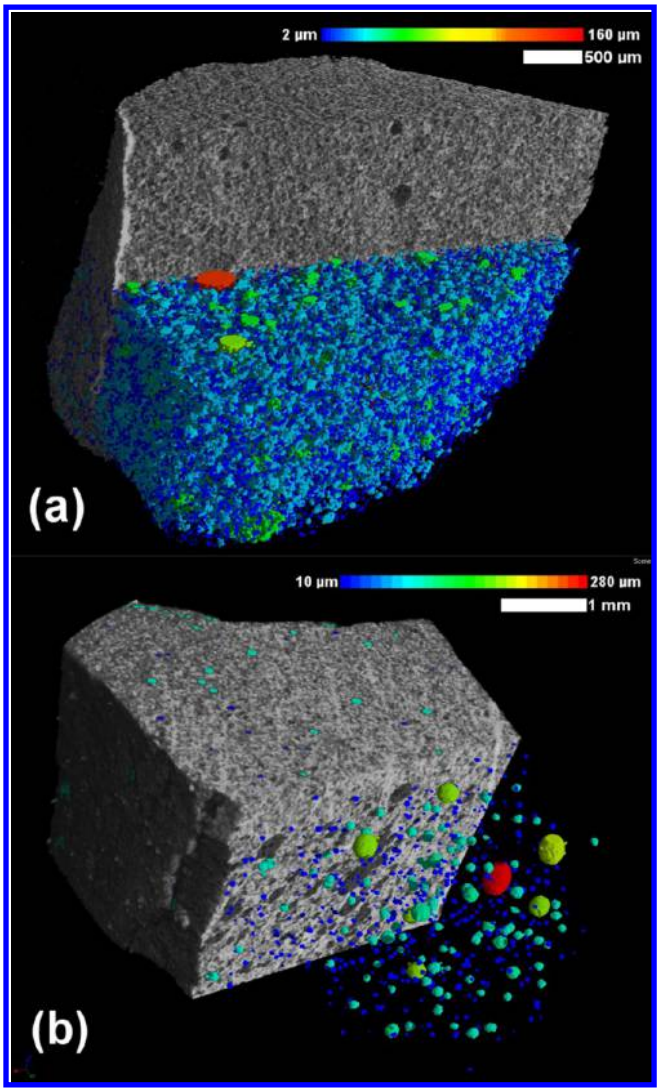

Figure 3. 3D renderings of X-ray computed tomography measurements, showing both the structure and the pore size analysis. Both volumes have been partially cut to improve visibility. The pores are color coded according to their equivalent diameter: (a) high-resolution scan; (b) low-resolution scan.

coded according to their equivalent diameter, which is the diameter of the sphere with the volume of the pore and as such a linearized scale for pore volume. The gray scale represents the local density in the voxel. In Figure 3a, the high-resolution scan is shown, giving information about pores of 2 μm and larger. Figure 3b shows the low-resolution scan, resolving only the pores larger than 10 μm equivalent diameter. The high resolution scan shows the widespread and large abundance of the smaller pores, with diameters from 2 to 10 μm, in agreement with the pore size distribution obtained by Hg-intrusion porosimetry. Conversely, the low-resolution scan helps to visualize the distribution of the larger pores, which are not as abundant as the smaller ones. The occurrence of larger pores is somewhat hidden in Figure 3a. The 3D scans confirm that a rather large pore size distribution is present in this sample, as already observed by the mercury intrusion porosimetry, and that pores are spatially well distributed inside the sample. The extremely low X-ray attenuation of this sample also points out to the high porosity of this sample, as shown by N_2 sorption data for micro- and mesopores, although the size of such pores cannot be quantitatively confirmed by X-ray tomography.

Besides a fully interconnected macroporous network, the carbonaceous foam reported herein presented mechanical properties good enough to enable carefree handling and shaping (Figure S1). After mercury intrusion porosimetry measurements, the materials used were still monolithic without showing any cracks. The monolithic foam was easily integrated in a membraneless purposely designed electrochemical reactor, as depicted in Figure S1. Interestingly, the inoculation and bioelectrochemical experiments could be performed in a continuous flow through the as-designed microcellular carbonaceous reactor. The electrode managed to withstand undamaged the constant pressure exerted by the continuous flow. The bear material showed a reasonable electrical conductivity of 10 S m^{-1}.

Figure 4 shows the catalytic current development from time of inoculation with anodic effluent from an existing BES

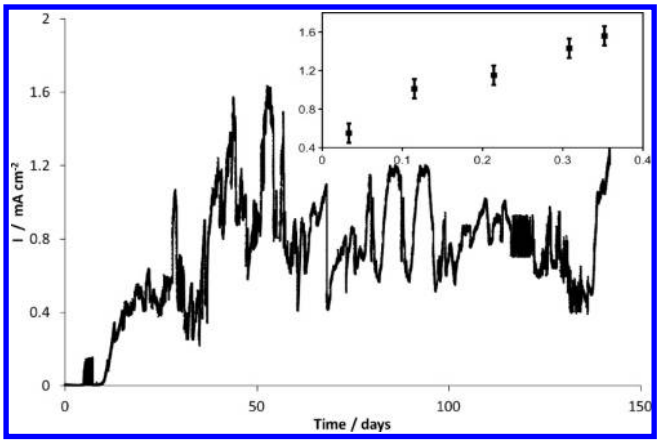

Figure 4. Bioelectrocatalytic current generation at a 750-HMF-CarboHIPE electrode in a continuous feed experiment. Biofilm derived from an anodic effluent and grown in artificial wastewater with 20 mM acetate and applied electrode potential of 0 V (vs Ag/AgCl). Varying flow rate as specified in the text. (inset) Catalytic current (mA cm^{-2}) vs flow rate (mL min^{-1}).

reactor. Catalytic current started to develop after 10 days. After 17 days, the current appeared to have reached a stationary value of 0.55 mA cm^{-2}. During 10 days the current remained at approximately constant values. Afterward the flow rate was increased from 0.033 to 0.115 mL min^{-1}, and a rather sharp current increase followed, with the current reaching 1.0 mA cm^{-2}. The flow rate was varied three more times to generate the current vs flow rate graph. The flow rate was maintained at 0.214 mL min^{-1} from day 57 until day 94, when it was further decreased for the remaining of the experiment to 0.115 mL min^{-1}. Some rather sharp fluctuations observed during the 150 days of the experiment are explained alternatively by either tubing leakages or clogging. These produced variations in substrate feeding rate, and eventually starved the biofilm during a few hours (usually during nighttime or weekends).

The inset in Figure 4 shows a linear behavior of the current density vs flow rate. The increase in current density with flow rate, suggests that the current is limited by either substrate delivery, protons removal, or both. Most likely the biofilm being relatively thick, most of the acetate is consumed and in practical terms, the current producing bacteria are not exposed to the bulk acetate concentration of 20 mM which should

DOI: 10.1021/acssuschemeng.5b01592
ACS Sustainable Chem. Eng. 2016, 4, 2508−2516

normally saturate the bacterial enzyme kinetics. Therefore, increasing the flow rate increases the rate of forced convection and hence the bacteria are exposed to higher acetate concentrations, which accelerate their metabolism. Moreover, a higher flow rate will help remove the protons from the vicinity of the biofilm and will help maintain neutral pH which will also increase the current density.

The catalytic current reached a maximum value of 1.56 mA cm^{-2} (normalization by projected surface area). When normalized in current per volume unit of electrode, this value translates to 7.8 mA cm^{-3} at the highest flow rate. Attempts to test higher flow rates were aborted because of repetitive issues with leakages when attempting to do so. Indeed, some of the sharp current decreases of Figure 4 were also due to these experimental issues (see above). An improved reactor design, would probably help reaching higher flow rates, developing higher catalytic currents, and possibly also overcome pore clogging (see below). For reference, two common commercially available electrodes, graphite felt and glassy carbon, developed bioelectrocatalytic currents of 0.8 ± 0.1 and 0.45 ± 0.05 mA cm^{-2} respectiviely, when operated under the same conditions and after inoculation with biological material from the same source, albeit in a different reactor.[36,37]

Figure 5 (full line) shows the CV in turnover conditions. The voltammogram exhibits the classic sigmoidal shape of electroactive biofilms under turnover conditions with some degree of hysteresis. The current starts to increase above −0.45 V and reaches a plateau of maximum current around 0.15 V. The plateau current is almost the same as the maximum current recorded in the chronoamperometry experiment at the same flow rate. A first derivative analysis (Figure S2) shows a symmetrical peak centered at −0.31 V (E_{hw}). The plateau current suggests that the maximum current is limited by either the enzymatic activity of acetate degradation, or diffusional limitations inside the three-dimensional electrode, i.e. arrival of acetate and diffusion of H^+ outside of the biofilm, and not by the interfacial kinetics of electron transfer. This hypothesis is in agreement with the discussion of the current vs flow rate graph. The onset potential for the start of the catalytic sigmoidal signal is governed by the redox potential of the redox moieties (be it soluble shuttles, membrane proteins or nanowires) interacting directly with the electrode surface. The wave shape and the onset potential are clear evidence of the microbial nature of the catalytic current, as has already been reported.[36,37,47,48] Moreover, the blank experiments, before microbial inoculation showed almost no current for the steady state chronoamperometry and no clear signal of faradaic reactions in the CV (dashed line in Figure 5). The onset potential for the turnover CV and the value of E_{hw}, together with the strong red color of our electrodes, see below, suggest that cytochromes are involved in the electron transfer from bacteria to electrode, although the detailed study of the electron transfer mechanism and the composition of the bacterial community are beyond the scope of this work.

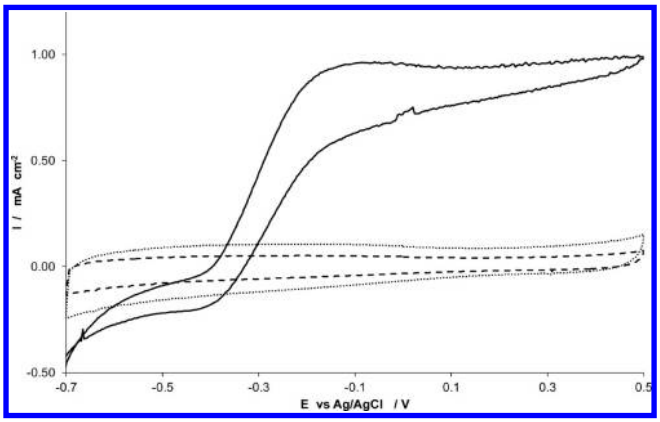

Figure 5. CVs recorded at 0.1 mV s^{-1}. (dashed line) Before inoculation, in the presence of 20 mM acetate. (full line) After 100 days of inoculation, 20 mM acetate. (dotted line) After 190 days of inoculation, no acetate.

At the end of the chronoamperometry experiment, the media in the reactor was replaced with fresh media without acetate. After 36 h of an applied potential in the absence of substrate, CVs were recorded in nonturnover conditions and are shown by the dotted line in Figure 5. The dashed curve shows for comparison the CV in abiotic conditions (before inoculation). No clear peaks or seemingly faradaic processes are seen in either the abiotic or the nonturnover CVs. Peaks in the nonturnover CV usually reveal the approximate redox potential of the species responsible for transferring electrons from the cells to the electrode. The apparent absence of these signals can be explained by the high nonfaradaic currents which are characteristic of porous electrodes. Nonturnover peaks are usually of much lower magnitude than turnover signals and in data presented here they are most probably hidden under the high capacitive currents.

Upon opening the reactors, the electrodes showed a reddish color on the upper surface, clearly distinctive to the naked eye. This is attributed to uniform biofilm coverage and suggests the presence of cytochromes.[36] Figure 6 shows SEM images of the biofilm developed in the inside and outside of the three-dimensional scaffold. Figure 6a shows a lateral view of the inside of the electrode (plane perpendicular to the cylinder base, and parallel to the fresh medium flow direction). The image was taken close to the center of the 2 mm thick electrode. We can observe a very thick biofilm coverage that has penetrated approximately the upper half of the cylinder. Surprisingly, the biofilm did not developed in the whole volume of the electrode. The profile of biofilm coverage stops quite abruptly and below a certain height, there is no evidence of biological activity. The biofilm is dense and thick, and it seems to block many of the pores. This porosity blockage is most probably at the origin of the partial coverage of the interior of the electrode. We hypothesize that the biofilm started to develop in the upper surface of the electrode and developed both toward the inside and the outside of the scaffold. Figure 6b is a top view of the upper surface of the electrode. On the left side of the image, a thick and rough biofilm surface is distinguished, while on the right side, salt deposits partially cover the underlying biofilm (due to incomplete washing).

Figure 6a and b together are proof of the generation of a thick and continuous biofilm in the whole upper surface and in the upper half of the interior of the monolith. Figure 6c is a zoom image on the same area as in Figure 6b, where several individual microbial shapes can be distinguished (bottom left). These appear to be rod-shaped and approximately 1 μm long.

DISCUSSION

The morphology of our monolithic material was thoroughly characterized combining nitrogen sorption, mercury porosimetry, SEM, and X-ray tomography. For X-ray tomography,

DOI: 10.1021/acssuschemeng.5b01592
ACS Sustainable Chem. Eng. 2016, 4, 2508−2516

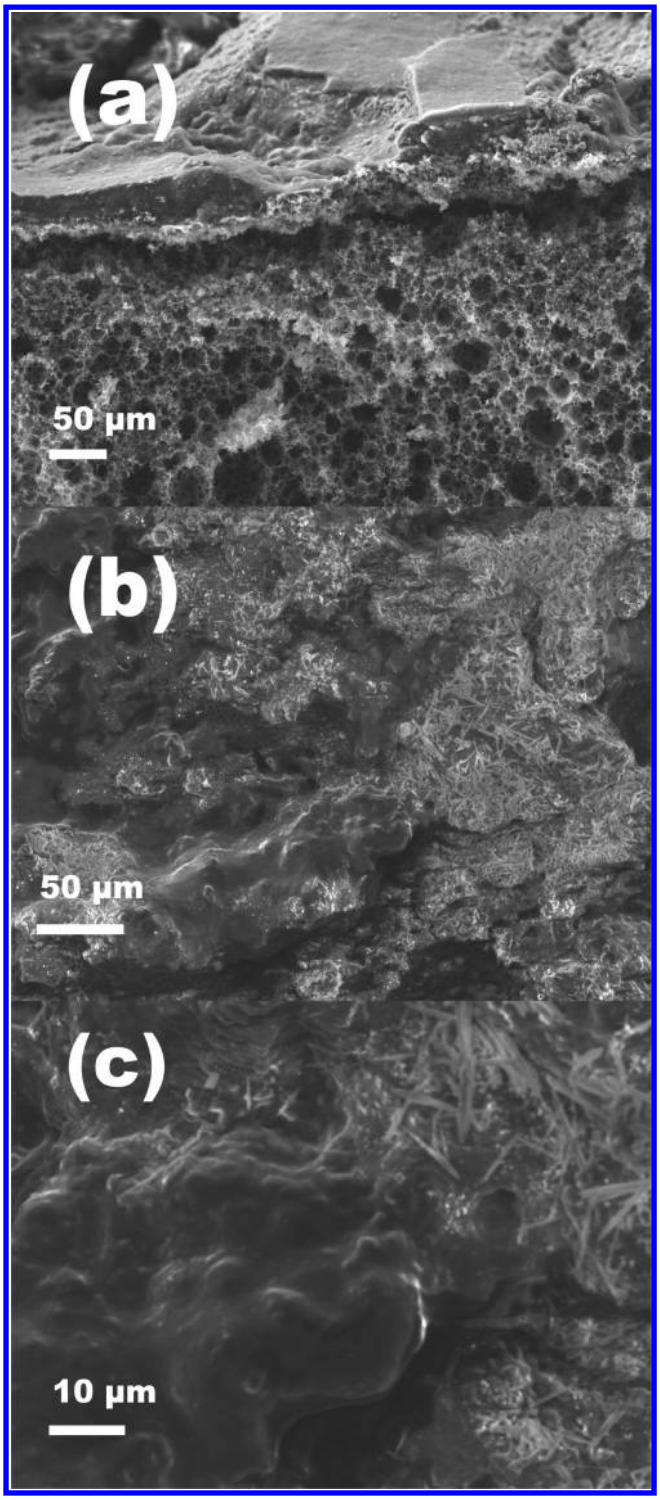

Figure 6. SEM micrographs after biofilm development. (a) Side view of the inner volume of the electrode (plane parallel to the flow direction). (b and c) Top of the electrode at different magnification (plane perpendicular to the flow direction).

gathering experimental data was not trivial, given that our samples are made almost exclusively from C, with smaller contributions of O and H, i.e. elements with very low X-ray attenuation. Moreover, these samples displayed a hierarchical porosity. Thus, these foams were shown to be both highly macroporous, with total pore volume of 9 $cm^3\ g^{-1}$ and porosity of more than 95% respectively, and micro−mesoporous, with BET surface area and total pore volume of 1130 $m^2\ g^{-1}$ and 0.43 $cm^3\ g^{-1,}$ respectively. Data shown in Figure 3 were only made available thanks to the accuracy of an in-house built setup which is noncommercially available. This is the first time that the spherical shape of the macroscopic pores (cells) of CarboHIPEs is experimentally observed. The 3D analysis also confirms the random distribution of pores sizes and occurrence along the whole volume of the material. From the 3D analysis, a porosity of approximately 20% is found to be due to pores larger than 2 μm. However, without quantitatively assessing a numeric value, the very low X-ray attenuation in the X-ray tomography analysis, very clearly hints toward a much higher porosity, similar to the porosity value indicated by Hg porositmetry (which takes into account pores from 10 nm to 100 μm). These features suggest that the smaller pores largely contribute to the porosity of the new material. Altogether, the data gathered here indicate the excellent complementarities of the different techniques used here to fully characterize the porosity of these samples.

The micro and mesopores of the 750-HMF-CarboHIPE are too small to contribute either to an increased available surface area for bacterial development or for improved liquid phase penetration inside the scaffold. However, we do believe that the nanometric features largely contributed to the high biocompatibility of this new material, providing a rough surface for bacterial attachment and connectivity for electron transfer.

It is very important to note that the catalytic current was stable for 6 months of continuous operation. After 6 months the reactor was stopped and the electrode was taken out for SEM analyses, i.e. most likely the reactor could have remained operational for longer periods. This stability points out once more toward the high biocompatibility of the new material. Even though pore clogging was evident, this fact did not affect continuous operation of the reactor.

The catalytic current values achieved are below several recent reports on new advanced materials for microbial anodes.[36,47−50] Today, the highest reported currents were achieved with extended macroporosity of 300 μm[36] and 1.4 mm.[47] A large quantity of macropores these sizes seem to be necessary to guarantee efficient mass transport of substrate toward the cells, and particularly to avoid accumulation of H^+ and local pH changes.[36,51] The macroporosity of our new material is below these values, with pores sizes on average extending up to 50 μm, and very few pores with diameters larger than 150 μm (Figures 2 and 3). In the case of a highly biocompatible material, such as the one we are analyzing, another current limiting factor at this low pore size is pore clogging, due to bacteria overgrowth. We believe that the current densities achieved are a consequence of the reduce pore sizes. Results presented here, take a new dimension when the synthetic route to the electrode materials is put forward: the precursors for the electrode synthesis come from biomass and from the bark of fruit trees, avoiding the use of toxic chemicals such as resorcinol, formaldehyde, divinylbenzene-based polymers, and the like. Still, the synthetic protocol is flexible enough to allow us to play around with the porosity distribution, which we plan to do in the future. Commercially available materials do not allow us to choose pores sizes; while other purposely designed materials for BES might show better current densities, but use more dangeours or toxic synthetic procedures.[36] All in all, we are confident that larger porosity while following a similar synthetic route will yield higher catalytic currents. Our data shows the high biocompatibility of the new materials as well as

DOI: 10.1021/acssuschemeng.5b01592
ACS Sustainable Chem. Eng. 2016, 4, 2508−2516

the long-term activity of the microbial communities within the scaffolds.

In summary, we have presented a new carbonaceous material which is fully biocompatible and a good candidate to be incorporated into microbial bioelectrochemical systems. Our new material was synthesized from biomass derived precursors, making an interesting sustainable cycle: biomass is used for the synthesis of electrodes where a biofilm can develop that will oxidize organic matter present in wastewater, generating electricity.

■ ASSOCIATED CONTENT

Supporting Information

The Supporting Information is available free of charge on the ACS Publications website at DOI: 10.1021/acssuschemeng.5b01592.

Pictures of the purposely designed bioelectrochemical reactor and electrode material; first derivative of turnover cyclic voltammogram (PDF)

■ AUTHOR INFORMATION

Corresponding Authors

*E-mail: vflexer@unju.edu.ar. Phone: (+54) 9388 4155 240 (V.F).

*E-mail: nicolas.Brun@enscm.fr. Phone: (+33) 4 67 16 34 66 (N.B.).

Present Addresses

○V.F.: Centro de Investigaciones y Transferencia−JUJUY Universidad Nacional de Jujuy-CONICET. Av. Bolivia 1239, San Salvador de Jujuy, 4600, Argentina.

△B.C.D.: The University of Queensland, School of Chemical Engineering, Level 3, Don Nicklin Building (74), Brisbane, QLD 4072, Australia.

Notes

The authors declare no competing financial interest.

■ ACKNOWLEDGMENTS

V.F. acknowledges a UQ Postdoctoral Fellowship. This work was supported by the Australian Research Council Grant DP110100539. The authors acknowledge the facilities and the scientific and technical assistance of the Australian Microscopy & Microanalysis Research Facility at the Centre for Microscopy and Microanalysis (The University of Queensland). The Ghent University Special Research Fund (BOF) is acknowledged for the postdoctoral grant of M.N.B.

■ REFERENCES

(1) Frackowiak, E.; Béguin, F. Carbon materials for the electrochemical storage of energy in capacitors. *Carbon* **2001**, *39* (6), 937−950.

(2) Candelaria, S. L.; Shao, Y.; Zhou, W.; Li, X.; Xiao, J.; Zhang, J. G.; Wang, Y.; Liu, J.; Li, J.; Cao, G. Nanostructured carbon for energy storage and conversion. *Nano Energy* **2012**, *1* (2), 195−220.

(3) Biener, J.; Stadermann, M.; Suss, M.; Worsley, M. A.; Biener, M. M.; Rose, K. A.; Baumann, T. F. Advanced carbon aerogels for energy applications. *Energy Environ. Sci.* **2011**, *4* (3), 656−667.

(4) Figueiredo, J. L. Functionalization of porous carbons for catalytic applications. *J. Mater. Chem. A* **2013**, *1* (33), 9351−9364.

(5) Wu, Z. Y.; Li, C.; Liang, H. W.; Chen, J. F.; Yu, S. H. Ultralight, flexible, and fire-resistant carbon nanofiber aerogels from bacterial cellulose. *Angew. Chem., Int. Ed.* **2013**, *52* (10), 2925−2929.

(6) Sevilla, M.; Fuertes, A. B.; Mokaya, R. High density hydrogen storage in superactivated carbons from hydrothermally carbonized renewable organic materials. *Energy Environ. Sci.* **2011**, *4* (4), 1400−1410.

(7) Tang, K.; Fu, L.; White, R. J.; Yu, L.; Titirici, M. M.; Antonietti, M.; Maier, J. Hollow carbon nanospheres with superior rate capability for sodium-based batteries. *Adv. Energy Mater.* **2012**, *2* (7), 873−877.

(8) Soorholtz, M.; White, R. J.; Zimmermann, T.; Titirici, M. M.; Antonietti, M.; Palkovits, R.; Schüth, F. Direct methane oxidation over Pt-modified nitrogen-doped carbons. *Chem. Commun.* **2013**, *49* (3), 240−242.

(9) Brun, N.; Edembe, L.; Gounel, S.; Mano, N.; Titirici, M. M. Emulsion-Templated Macroporous Carbons Synthesized by Hydrothermal Carbonization and their Application for the Enzymatic Oxidation of Glucose. *ChemSusChem* **2013**, *6* (4), 701−710.

(10) Yang, W.; Fellinger, T. P.; Antonietti, M. Efficient metal-free oxygen reduction in alkaline medium on high-surface-area mesoporous nitrogen-doped carbons made from ionic liquids and nucleobases. *J. Am. Chem. Soc.* **2011**, *133* (2), 206−209.

(11) Flexer, V.; Brun, N.; Courjean, O.; Backov, R.; Mano, N. Porous mediator-free enzyme carbonaceous electrodes obtained through integrative chemistry for biofuel cells. *Energy Environ. Sci.* **2011**, *4* (6), 2097−2106.

(12) Brun, N.; Osiceanu, P.; Titirici, M. M. Biosourced nitrogen-doped microcellular carbon monoliths. *ChemSusChem* **2014**, *7* (2), 397−401.

(13) Brun, N.; Ungureanu, S.; Deleuze, H.; Backov, R. Hybrid foams, colloids and beyond: From design to applications. *Chem. Soc. Rev.* **2011**, *40* (2), 771−788.

(14) Gao, H.; Pan, J.; Han, D.; Zhang, Y.; Shi, W.; Zeng, J.; Peng, Y.; Yan, Y. Facile synthesis of microcellular foam catalysts with adjustable hierarchical porous structure, acid-base strength and wettability for biomass energy conversion. *J. Mater. Chem. A* **2015**, *3* (25), 13507−13518.

(15) Zhang, Y.; Pan, J.; Chen, Y.; Shi, W.; Yan, Y.; Yu, L. HIPEs template: Towards the synthesis of polymeric catalysts with adjustable porous structure, acid-base strength and wettability for biomass energy conversation. *Chem. Eng. J.* **2016**, *283*, 956−970.

(16) Titirici, M.; White, R.; Falco, C.; Sevilla, M. Black perspectives for a green future: hydrothermal carbons for environment protection and energy storage. *Energy Environ. Sci.* **2012**, *5*, 6796−6822.

(17) Titirici, M.; Antonietti, M. Chemistry and materials options of sustainable carbon materials made by hydrothermal carbonization. *Chem. Soc. Rev.* **2010**, *39*, 103−116.

(18) Rabaey, K., Angenent, L., Schröder, U., Keller, J., Eds. *Bioelectrochemical Systems: From Extracellular Electron Transfer to Biotechnological Applications*; IWA Publishing: London, 2010.

(19) Logan, B. E. Exoelectrogenic bacteria that power microbial fuel cells. *Nat. Rev. Microbiol.* **2009**, *7* (5), 375−381.

(20) Lovley, D. R. Bug juice: Harvesting electricity with microorganisms. *Nat. Rev. Microbiol.* **2006**, *4* (7), 497−508.

(21) Jourdin, L.; Freguia, S.; Donose, B. C.; Chen, J.; Wallace, G. G.; Keller, J.; Flexer, V. A novel carbon nanotube modified scaffold as an efficient biocathode material for improved microbial electrosynthesis. *J. Mater. Chem. A* **2014**, *2* (32), 13093−13102.

(22) Jourdin, L.; Grieger, T.; Monetti, J.; Flexer, V.; Freguia, S.; Lu, Y.; Chen, J.; Romano, M.; Wallace, G. G.; Keller, J. High Acetic Acid Production Rate Obtained by Microbial Electrosynthesis from Carbon Dioxide. *Environ. Sci. Technol.* **2015**, *49* (22), 13566−13574.

(23) Patil, S. A.; Arends, J. B. A.; Vanwonterghem, I.; Van Meerbergen, J.; Guo, K.; Tyson, G. W.; Rabaey, K. Selective Enrichment Establishes a Stable Performing Community for Microbial Electrosynthesis of Acetate from CO_2. *Environ. Sci. Technol.* **2015**, *49* (14), 8833−8843.

(24) Tremblay, P. L.; Zhang, T. Electrifying microbes for the production of chemicals. *Front. Microbiol.* **2015**, *6* (MAR), 201.

(25) Harnisch, F.; Rosa, L. F. M.; Kracke, F.; Virdis, B.; Krömer, J. O. Electrifying white biotechnology: Engineering and economic potential of electricity-driven bio-production. *ChemSusChem* **2015**, *8* (5), 758−766.

DOI: 10.1021/acssuschemeng.5b01592
ACS Sustainable Chem. Eng. 2016, 4, 2508−2516

(26) Rozendal, R. A.; Hamelers, H. V. M; Rabaey, K.; Keller, J.; Buisman, C. J. N. Towards practical implementation of bioelectrochemical wastewater treatment. *Trends Biotechnol.* **2008**, *26* (8), 450−459.
(27) Krieg, T.; Sydow, A.; Schröder, U.; Schrader, J.; Holtmann, D. Reactor concepts for bioelectrochemical syntheses and energy conversion. *Trends Biotechnol.* **2014**, *32* (12), 645−655.
(28) Guo, K.; Prévoteau, A.; Patil, S. A.; Rabaey, K. Engineering electrodes for microbial electrocatalysis. *Curr. Opin. Biotechnol.* **2015**, *33*, 149−156.
(29) Higgins, S. R.; Foerster, D.; Cheung, A.; Lau, C.; Bretschger, O.; Minteer, S. D.; Nealson, K.; Atanassov, P.; Cooney, M. J. Fabrication of macroporous chitosan scaffolds doped with carbon nanotubes and their characterization in microbial fuel cell operation. *Enzyme Microb. Technol.* **2011**, *48* (6−7), 458−465.
(30) Xie, X.; Hu, L.; Pasta, M.; Wells, G. F.; Kong, D.; Criddle, C. S.; Cui, Y. Three-dimensional carbon nanotube-textile anode for high-performance microbial fuel cells. *Nano Lett.* **2011**, *11* (1), 291−296.
(31) Xie, X.; Ye, M.; Hu, L.; Liu, N.; McDonough, J. R.; Chen, W.; Alshareef, H. N.; Criddle, C. S.; Cui, Y. Carbon nanotube-coated macroporous sponge for microbial fuel cell electrodes. *Energy Environ. Sci.* **2012**, *5* (1), 5265−5270.
(32) Mink, J. E.; Rojas, J. P.; Logan, B. E.; Hussain, M. M. Vertically Grown Multiwalled Carbon Nanotube Anode and Nickel Silicide Integrated High Performance Microsized (1.25 μL) Microbial Fuel Cell. *Nano Lett.* **2012**, *12* (2), 791−795.
(33) Zhao, Y.; Watanabe, K.; Nakamura, R.; Mori, S.; Liu, H.; Ishii, K.; Hashimoto, K. Three-dimensional conductive nanowire networks for maximizing anode performance in microbial fuel cells. *Chem. - Eur. J.* **2010**, *16* (17), 4982−4985.
(34) Patil, S. A.; Chigome, S.; Hägerhäll, C.; Torto, N.; Gorton, L. Electrospun carbon nanofibers from polyacrylonitrile blended with activated or graphitized carbonaceous materials for improving anodic bioelectrocatalysis. *Bioresour. Technol.* **2013**, *132*, 121−126.
(35) Kipf, E.; Koch, J.; Geiger, B.; Erben, J.; Richter, K.; Gescher, J.; Zengerle, R.; Kerzenmacher, S. Systematic screening of carbon-based anode materials for microbial fuel cells with Shewanella oneidensis MR-1. *Bioresour. Technol.* **2013**, *146*, 386−392.
(36) Flexer, V.; Chen, J.; Donose, B. C.; Sherrell, P.; Wallace, G. G.; Keller, J. The nanostructure of three-dimensional scaffolds enhances the current density of microbial bioelectrochemical systems. *Energy Environ. Sci.* **2013**, *6* (4), 1291−1298.
(37) Flexer, V.; Marque, M.; Donose, B. C.; Virdis, B.; Keller, J. Plasma treatment of electrodes significantly enhances the development of anodic electrochemically active biofilms. *Electrochim. Acta* **2013**, *108*, 566−574.
(38) Dennis, P. G.; Guo, K.; Imelfort, M.; Jensen, P.; Tyson, G. W.; Rabaey, K. Spatial uniformity of microbial diversity in a continuous bioelectrochemical system. *Bioresour. Technol.* **2013**, *129*, 599−605.
(39) Rabaey, K.; Ossieur, W.; Verhaege, M.; Verstraete, W. Continuous microbial fuel cells convert carbohydrates to electricity. *Water Sci. Technol.* **2005**, *52*, 515−523.
(40) Thommes, M.; Kaneko, K.; Neimark, A. V.; Olivier, J. P.; Rodriguez-Reinoso, F.; Rouquerol, J.; Sing, K. S. W. Physisorption of gases, with special reference to the evaluation of surface area and pore size distribution (IUPAC Technical Report). *Pure Appl. Chem.* **2015**, *87* (9−10), 1051−1069.
(41) Washburn, E. W. The Dynamics of Capillary Flow. *Phys. Rev.* **1921**, *17*, 273−283.
(42) Rouquerol, J.; Baron, G.; Denoyel, R.; Giesche, H.; Groen, J.; Klobes, P.; Levitz, P.; Neimark, A. V.; Rigby, S.; Skudas, R.; Sing, K.; Thommes, M.; Unger, K. Liquid intrusion and alternative methods for the characterization of macroporous materials (IUPAC technical report). *Pure Appl. Chem.* **2011**, *84* (1), 107−136.
(43) Groso, A.; Abela, R.; Stampanoni, M. Implementation of a fast method for high resolution phase contrast tomography. *Opt. Express* **2006**, *14* (18), 8103−8110.
(44) Boone, M. N.; De Witte, Y.; Dierick, M.; Almeida, A.; Van Hoorebeke, L. Improved signal-to-noise ratio in laboratory-based phase contrast tomography. *Microsc. Microanal.* **2012**, *18* (2), 399−405.
(45) Brabant, L.; Vlassenbroeck, J.; De Witte, Y.; Cnudde, V.; Boone, M. N.; Dewanckele, J.; Van Hoorebeke, L. Three-dimensional analysis of high-resolution X-ray computed tomography data with morpho+. *Microsc. Microanal.* **2011**, *17* (2), 252−263.
(46) Almeida, A.; Possemiers, S.; Boone, M. N.; De Beer, T.; Quinten, T.; Van Hoorebeke, L.; Remon, J. P.; Vervaet, C. Ethylene vinyl acetate as matrix for oral sustained release dosage forms produced via hot-melt extrusion. *Eur. J. Pharm. Biopharm.* **2011**, *77* (2), 297−305.
(47) Chen, S.; He, G.; Liu, Q.; Harnisch, F.; Zhou, Y.; Chen, Y.; Hanif, M.; Wang, S.; Peng, X.; Hou, H.; Schroeder, U. Layered corrugated electrode macrostructures boost microbial bioelectrocatalysis. *Energy Environ. Sci.* **2012**, *5*, 9769−9772.
(48) Chen, S.; Hou, H.; Harnisch, F.; Patil, S. A.; Carmona-Martinez, A. A.; Agarwal, S.; Zhang, Y.; Sinha-Ray, S.; Yarin, A. L.; Greiner, A.; Schroder, U. Electrospun and solution blown three-dimensional carbon fiber nonwovens for application as electrodes in microbial fuel cells. *Energy Environ. Sci.* **2011**, *4* (4), 1417−1421.
(49) Katuri, K.; Ferrer, M. L.; Gutiérrez, M. C.; Jiménez, R.; Del Monte, F.; Leech, D. Three-dimensional microchanelled electrodes in flow-through configuration for bioanode formation and current generation. *Energy Environ. Sci.* **2011**, *4* (10), 4201−4210.
(50) Yuan, Y.; Zhou, S.; Liu, Y.; Tang, J. Nanostructured Macroporous Bioanode Based on Polyaniline-Modified Natural Loofah Sponge for High-Performance Microbial Fuel Cells. *Environ. Sci. Technol.* **2013**, *47* (24), 14525−14532.
(51) Torres, C. I.; Marcus, A. K.; Rittmann, B. E. Proton transport inside the biofilm limits electrical current generation by anode-respiring bacteria. *Biotechnol. Bioeng.* **2008**, *100* (5), 872−881.

DOI: 10.1021/acssuschemeng.5b01592
ACS Sustainable Chem. Eng. 2016, 4, 2508−2516